Testing One Hypothesis Multiple Times

Sara Algeri[1,2] and David A. van Dyk[2]

[1]*University of Minnesota* and [2]*Imperial College London*

Abstract: In applied settings, hypothesis testing when a nuisance parameter is identifiable only under the alternative often reduces to a problem of *testing one hypothesis multiple times* (TOHM). Specifically, a fine discretization of the space of the nonidentifiable parameter is specified, and the null hypothesis is tested against a set of *sub-alternative hypotheses*, one for each point of the discretization. The resulting *sub-test statistics* are then combined to obtain a *global p-value*. We propose a computationally efficient inferential tool to perform TOHM under stringent significance requirements, such as those typically required in the physical sciences, (e.g., a p-value $< 10^{-7}$). The resulting procedure leads to a generalized approach to performing inferences under nonstandard conditions, including non-nested model comparisons.

Key words and phrases: Multiple hypothesis testing, bump hunting, non-identifiabily in hypothesis testing, non-nested models comparison.

1. Introduction

A fundamental statistical challenge in scientific discoveries is the so-called "bump-hunting" problem (Choudalakis, 2011), where researchers aim to

distinguish peaks due to a signal of interest (the new discovery) from peaks due to random fluctuations of the background. In the framework of hypothesis testing, the null model specified by H_0 is typically the background-only model, and a signal bump is added in the alternative model specified by H_1. Consider, for example, a dark matter search. Here, we aim to distinguish events from a background that follows a power-law (Pareto type-I) distribution from the signal of a dark matter source, modeled as a narrow Gaussian bump, with an unknown location, over the search area $\Theta \equiv [\mathcal{L}, \mathcal{U}] \subset \mathbb{R}$. We can specify the model of interest using a mixture model,

$$(1 - \eta)\frac{1}{k_\phi y^{\phi+1}} + \frac{\eta}{k_\theta} \exp\left\{-\frac{(y - \theta)^2}{0.02\theta^2}\right\} \qquad \text{for } y \geq 1, \qquad (1.1)$$

where k_ϕ and k_θ are normalizing constants, for $y \geq 1$, $\phi > 0$, and $\theta \geq 1$. Note that the parameter θ characterizes both the location of the signal over the search region and its standard deviation. Specifically, the bump becomes wider as its position moves further into the tail of the background distribution. The model in (1.1) simplifies those models involved in searches for γ-ray emissions in a cluster of galaxies (Anderson et al., 2016), where, for example, the width of the signal may be a more complex function of its location. Despite its simplicity, the model in (1.1) introduces the key

statistical issues arising in the context of dark matter searches, as described below.

In order to assess the evidence in favor of the signal, we test

$$H_0 : \eta = 0 \quad \text{versus} \quad H_1 : \eta > 0. \qquad (1.2)$$

where η is the proportion of events due to the dark matter emission and, typically, $0 \leq \eta \leq 1$. Despite its straightforward formulation, testing (1.2) is nontrivial. Difficulties arise because θ is not defined under H_0. Consequently, the classical asymptotic properties of, for example, the maximum lixelihood estimates (MLE) and the likelihood ratio test (LRT) fail. Analogously, complications may arise when using resampling techniques, such as bootstrapping (Efron and Tibshirani, 1994), to derive the null distribution of the test statistic in the presence of stringent significance requirements. For searches in high energy physics, for instance, the significance level necessary to claim a discovery can be in the order of 10^{-7} (see Lyons, 2013, Table 1). Hence, a large (e.g., $O(10^8)$) simulation may be infeasible when dealing with complex models. This is a key motivation for a computationally efficient inferential solution.

To address these difficulties, we consider the bump-hunting problem

as a special case of what is known in the statistical literature as *"testing statistical hypotheses when a nuisance parameter is present only under the alternative."* In addition to bump-hunting, classical examples may include regression models in which structural changes, such as break-points and threshold-effects, occur (Andrews, 1993; Hansen, 1992b, 1999; Davies, 2002).

The general problem is well documented, starting at least from the seminal works of Hotelling (1939) and Davies (1977, 1987), and investigated further in the econometrics literature by several authors, including Andrews and Ploberger (1994) and Hansen (1991, 1992a, 1996). In their practical implementations, these methods reduce the problem of testing with unidentifiable parameters under H_0 to one of *testing one hypothesis multiple times* (TOHM). Here, a single null hypothesis H_0 is tested against different *sub-alternative hypotheses* of the form $H_1(\theta)$, one for each fixed θ in Θ, and a corresponding ensemble of *sub-test statistics*, indexed by θ, namely $W(\theta)$, is specified. The goal is to provide a global p-value as the standard of evidence for comparing H_0 and the global alternative hypothesis H_1, of which each $H_1(\theta)$ is a special case. Unfortunately, existing methods often require case-by-case mathematical computations (e.g., Davies, 1977), estimating the covariance structure (e.g., Hansen, 1991), choosing weight-

ing functions (e.g., Andrews and Ploberger, 1994), or full simulations of the empirical process (e.g., Hansen, 1992a, 1996).

As such, we propose a computationally efficient method to perform TOHM that overcomes these limitations. Specifically, as in Davies (1977, 1987), we consider a stochastic process, $\{W(\theta)\}$, indexed by $\theta \in \Theta \equiv [\mathcal{L}, \mathcal{U}]$, and with covariance function $\rho(\theta, \theta^{\dagger})$. We consider the global p-value

$$P\left(\sup_{\theta \in \Theta}\{W(\theta)\} > c\right), \tag{1.3}$$

where c is the observed value of the *global test statistic*, $\sup_{\theta \in \Theta}\{W(\theta)\}$. The central difficulty of this approach is to derive or approximate (1.3). One option is to employ extreme value theory (EVT), as in Cramér and Lead-better (2013, p. 272), where a bound for (1.3) is obtained by considering the upcrossings of c by $\{W(\theta)\}$ (see Figure S.1). Specifically, $\{W(\theta)\}$ has an *upcrossing* of a threshold $c \in \mathbb{R}$ at $\theta_0 \in \Theta$ if, for some $\epsilon > 0$, $W(\theta) \leq c$ in the interval $(\theta_0 - \epsilon, \theta_0)$, and $W(\theta) \geq c$ in the interval $[\theta_0, \theta_0 + \epsilon)$ (Adler, 2000). Let N_c be the number of upcrossings of c by $\{W(\theta)\}$. Using Markov's inequality, Cramér and Leadbetter (2013, p. 272) show that (1.3) can be

bounded as in (1.4),

$$P\left(\sup_{\theta\in\Theta}\{W(\theta)\} > c\right) \le P(W(\mathcal{L}) > c) + E[N_c], \qquad (1.4)$$

where $P(W(\mathcal{L}) > c)$ is typically known. Davies (1977, 1987) considers cases where $\{W(\theta)\}$ is a Gaussian or a χ^2 process, estimates $E[N_c]$ using total variation, and shows that (1.4) becomes sharp as $c \to \infty$ (under long-range independence, i.e., if $\rho(\theta, \theta^\dagger) \to 0$ as $|\theta - \theta^\dagger| \to \infty$). Unfortunately, Hansen (1991) points out that situations exist where the total variation diverges.

An alternative solution can overcome this problem, and has had a significant impact in physics (Gross and Vitells, 2010). Consider a set of observations $y_1, \ldots, y_n$, and let $T_n(\theta)$ be the LRT statistic used to test (1.2), evaluated on $y_1, \ldots, y_n$ when θ is fixed. We denote the LRT process indexed by different values of θ as $\{T_n(\theta)\}$. Under H_0 and suitable uniformity conditions (Hansen, 1991), $\{T_n(\theta)\} \xrightarrow[n\to\infty]{d} \{W_\chi(\theta)\}$, where $W_\chi(\theta)$ is a χ^2 process with components $W_\chi(\theta) \sim \chi_s^2$, for each $\theta \in [\mathcal{L}, \mathcal{U}]$ fixed. Let $E[N_c^\chi]$ be the expected number of upcrossings of c by $\{W_\chi(\theta)\}$ over Θ. One possible way to compute (1.4) is to estimate $E[N_c^\chi]$ using Monte Carlo simulations. However, when dealing with stringent significance requirements, the corresponding significance threshold c is typically very large. Hence,

upcrossings of c are expected to occur infrequently when simulating under H_0 and, thus, a massive simulation is required to estimate $E[N_c^\chi]$ directly. Gross and Vitells (2010) exploit the χ^2 distribution of $\{W_\chi(\theta)\}$ to rewrite $E[N_c^\chi]$ as a function of $E[N_{c_0}^\chi]$ for some $c_0 << c$:

$$P\left(\sup_{\theta \in \Theta}\{W_\chi(\theta)\} > c\right) \le P(W_\chi(\mathcal{L}) > c) + \left(\frac{c}{c_0}\right)^{\frac{s-1}{2}} e^{-\frac{c-c_0}{2}} E[N_{c_0}^\chi]. \qquad (1.5)$$

where $E[N_c^\chi] = \left(\frac{c}{c_0}\right)^{\frac{s-1}{2}} e^{-\frac{c-c_0}{2}} E[N_{c_0}^\chi]$. This allows a drastic reduction in the computational effort needed to compute $E[N_c^\chi]$. Specifically, upcrossings of $c_0 << c$ are expected to occur often, thus, $E[N_{c_0}^\chi]$ can be estimated accurately using a small Monte Carlo simulation.

Gross and Vitells (2010) do not formally justify (1.5). In Section 2, we derive (1.5), generalize it to any process $\{W(\theta)\}$, and clarify the conditions under it and its generalization hold. Efficient choices of c_0 are discussed in Section 3, and a simple graphical tool is proposed to validate the adequacy of the number of sub-tests conducted.

The resulting procedure leads to a generalized approach for performing inferences under nonstandard regularity conditions, including, as discussed in Section 3, comparisons of non-nested models. This can be done by specifying a comprehensive model that includes the two (non-nested) models

being compared as special cases. We then perform two hypothesis tests of hypothesis where a nuisance parameter is present only under the alternative to evaluate the two models (Algeri et al., 2016).

In principle, the problem of testing in the presence of a nuisance parameter that is present only under the alternative can be formulated as a multiple hypothesis testing (MHT) problem. Here, several tests are conducted over a grid of possible values of θ, and corrected using Bonferroni's correction (Bonferroni, 1935, 1936), or similar methods, to control for the probability of a type-I error. Although the Bonferroni correction is easy to implement, it is often dismissed by practitioners because of its stringent control of the overall false detection rate and its artificial dependence on the number of tests conducted. In Section 4, we compare TOHM and Bonferroni's correction using numerical studies and data applications. Here, we discuss how the proposed tools can be used to identify situations where, by virtue of its relationship with TOHM, Bonferroni can be used without being concerned about obtaining an overly conservative result.

The remainder of the paper is organized as follows. In Section 2, we define the TOHM framework, and derive a computable upper bound for (1.3) by generalizing (1.5). In Section 3, we illustrate how TOHM can be used to distinguish between non-nested models, validate our results using

simulation studies, and discuss graphical tools for selecting the necessary
quantities in the computation of the bound proposed in Section 2. In Sec-
tion 4, we investigate the relationship between TOHM and the classical
Bonferroni correction, and apply both methods to several realistic data
sets. Section 5 concludes the paper. Additional figures, data, and proofs
are collected in the online Supplementary Material.

2. TOHM via EVT

2.1 Definition and formalization

In this section, we generalize the testing procedure of Gross and Vitells
(2010) beyond the LRT and the χ^2 case to formalize it in statistical terms.
This allows us to establish a general theoretical framework to efficiently
bound/approximate the global p-value in (1.3).

Recall that $\{W(\theta)\}$ is a generic stochastic process indexed by $\theta \in \Theta \equiv$
$[\mathcal{L}; \mathcal{U}]$, with covariance function $\rho(\theta, \theta^\dagger)$. Following Davies (1987), we stip-
ulate the following condition.

Condition 1. $\{W(\theta)\}$ *has continuous sample paths, it has a continuous*
first derivative, except possibly for a finite number of jumps, and its com-
ponents $W(\theta)$ are identically distributed, for all $\theta \in \Theta$.

To exploit (1.4), we aim to conveniently estimate $E[N_c]$ and bound or
approximate (1.3). Results 2 and 3 allow this.

Result 2. *Let $c \in \mathbb{R}$ be an arbitrary threshold, let $a(c)$ be a function that depends on c, but not on θ, and let $b(\Theta)$ be a function calculated over Θ that does not depend on c. Under Condition 1, if $E[N_c]$ can be decomposed as*

$$E[N_c] = a(c)b(\Theta), \tag{2.6}$$

then

$$E[N_c] = \frac{a(c)}{a(c_0)}E[N_{c_0}] \qquad \forall c_0 \leq c, c_0 \in \mathbb{R}. \tag{2.7}$$

The function $b(\Theta)$ typically involves integration over the interval Θ, and should not be confused with a function of θ. Deriving a closed-form expression of $b(\Theta)$ in (2.6) may be challenging, and may require knowledge of $\rho(\theta, \theta^\dagger)$. Conversely, the form of $a(c)$ typically depends on the marginal distribution of the components $W(\theta)$ of $\{W(\theta)\}$, hence the requirement of an identical distribution in Condition 1. The continuity assumptions on $\{W(\theta)\}$ and its first derivative prevent $E[N_c]$ from diverging.

Equation (2.7) offers a simple way to compute $E[N_c]$, provided that, as discussed below, $E[N_{c_0}]$ can be estimated accurately. Result 3 follows from (1.4), (2.6), and (2.7).

Result 3. *Under Condition 1, if* (2.6) *holds,* (1.3) *can be bounded by*

$$
P\left(\sup_{\theta \in \Theta}\{W(\theta)\} > c\right) \le P(W(\mathcal{L}) > c) + \frac{a(c)}{a(c_0)}E[N_{c_0}], \qquad (2.8)
$$

for all $c_0 \le c, c_0 \in \mathbb{R}$. *In addition, if* $\rho(\theta, \theta^\dagger) \to 0$ *as* $|\theta - \theta^\dagger| \to \infty$, *the difference between the left- and the right-hand side of* (2.8) *approaches zero as* $c \to \infty$.

2.2   TOHM bounds for Gaussian-related processes

The bound in (1.5) and analogous bounds for Gaussian and related processes, such as F and t processes, can be derived using results from random fields theory, as discussed in Algeri and van Dyk (2019). In this setting, it can be shown that, under mild smoothness conditions (see Taylor and Adler (2003, p. 547)), $E[N_c]$ enjoys the decomposition in (2.6). Here, $a(c)$ depends only on the distribution of the marginals of $\{W(\theta)\}$, whereas $b(\Theta)$ corresponds to the so-called Lipschitz Killing curvature of first order (e.g., Adler and Taylor, 2009), and is typically difficult to compute. We report explicit forms of the right-hand side of (2.8) for the Gaussian, F, and t processes obtained from these results (see Taylor and Worsley, 2008; Adler and Taylor, 2009; Algeri and van Dyk, 2019, for more details).

2.2 TOHM bounds for Gaussian-related processes

Gaussian process. Let $\{Z(\theta)\}$ be a mean zero and variance one Gaussian process, such that $Z(\theta) \sim N(0,1)$, for all $\theta \in \Theta$, and let N_c^Z be the process of upcrossings of c_0 by $\{Z(\theta)\}$ over $\Theta \equiv [\mathcal{L}, \mathcal{U}]$. The TOHM bound in equation (2.8) takes the form

$$P\left(\sup_{\theta \in \Theta}\{Z(\theta)\} \geq c\right) \leq \Phi(-c) + e^{-\frac{c^2 - c_0^2}{2}} E[N_{c_0}^Z], \qquad (2.9)$$

where $\Phi(-c)$ is the cumulative density function of a standard normal random variable evaluated at $-c$, and the ratio $\frac{a(c)}{a(c_0)}$ is given by $e^{-\frac{c^2 - c_0^2}{2}}$. For the stationary case, the same result can be obtained by expressing $E[N_c^Z]$ using Rice's formula (Rice, 1944), that is,

$$E[N_c^Z] = \frac{|\mathcal{L} - \mathcal{U}|}{2\pi}\sqrt{\rho''(\theta, \theta)}e^{-\frac{c^2}{2}}$$

where $\rho''(\theta, \theta) = \frac{\partial \theta}{\partial \theta \partial \theta^\dagger}\rho(\theta, \theta^\dagger)\big|_{\theta^\dagger = \theta}$ is the second spectral moment of $\{Z(\theta)\}$ and is assumed to be finite, and $|\mathcal{L} - \mathcal{U}|$ is the length of Θ. As discussed in Davies (1987), for a two-sided test, the excursion probability of interest is $P(\sup_{\theta \in \Theta} |\{Z(\theta)\}| \geq c)$, the bound of which is twice the right-hand side of (2.9).

The rates of convergence of the difference between the right- and left-hand sides of (1.5) and (2.9) are discussed in Section S.1 of the Supplemen-

tary Material. In Section 3, we further study the sharpness of the bounds

in (1.5) and (2.9) as $c \to \infty$ using simulation studies.

F **process.**   Consider an F process $\{F(\theta)\}$ with s and v degrees of free-

dom, such that $F(\theta) \sim F_{s,v}$, for all $\theta \in \Theta$. Let $E[N_{c_0}^F]$ be the expected

number of upcrossings of c_0 by $\{F(\theta)\}$. Then the TOHM bound in equa-

tion (2.8) takes the form

$$
P\left(\sup_{\theta \in \Theta}\{F(\theta)\} \geq c\right) \leq P(F(\mathcal{L}) \geq c) + \left(\frac{c}{c_0}\right)^{\frac{s-1}{2}} \left(\frac{v + s \cdot c}{v + s \cdot c_0}\right)^{-\frac{s+v-2}{2}} E[N_{c_0}^F],
$$

$$(2.10)$$

for all $c_0 \leq c, c_0 \in \mathbb{R}$, and with $a(c) = c^{\frac{s-1}{2}} (v + s \cdot c)^{-\frac{s+v-2}{2}}$.

t **process.**   Consider a t process $\{V(\theta)\}$ with s degrees of freedom, such

that $V(\theta) \sim t_s$. Let $E[N_{c_0}^V]$ be the expected number of upcrossings of c_0 by

$\{V(\theta)\}$. Then the TOHM bound in equation (2.8) takes the form

$$
P\left(\sup_{\theta \in \Theta}\{V(\theta)\} \geq c\right) \leq P(V(\mathcal{L}) \geq c) + \left(\frac{1 + c^2}{1 + c_0^2}\right)^{-\frac{s-1}{2}} E[N_{c_0}^V], \qquad (2.11)
$$

for all $c_0 \leq c, c_0 \in \mathbb{R}$, and with $a(c) = (1 + c^2)^{-\frac{s-1}{2}}$.

2.3   TOHM in practice

In practice, we evaluate $\{W(\theta)\}$ on a fine grid of points, namely $\Theta_R = \{\theta_1, \ldots \theta_R\} \subseteq \Theta$, with R being the typically large number of grid points. Let $\{W(\theta_r)\}$ be the random sequence that coincides with $\{W(\theta)\}$ at each $\theta_r \in \Theta_R$, and let $\{w(\theta_r)\}$ be its observed value. We approximate $\sup_{\theta \in \Theta}\{W(\theta)\}$ using its discrete counterpart $\max_{\theta_r \in \Theta_R}\{W(\theta_r)\}$, the observed value of which is given by

$$c_R = \max_{\theta_r \in \Theta_R}\{w(\theta_r)\}. \tag{2.12}$$

Let the process of upcrossings of c_R by $\{W(\theta_r)\}$, namely $\tilde{N}_{c_R}$, be events of the type $\{W(\theta_{r-1}) \leq c_R, W(\theta_r) > c_R\}$. We assume Θ_R is sufficiently dense, such that the right-hand side of (2.8) can be approximated by (2.13), as $R \to \infty$,

$$P(W(\mathcal{L}) > c_R) + \frac{a(c_R)}{a(c_0)} E[\tilde{N}_{c_0}] \qquad \forall c_0 \leq c_R, c_0 \in \mathbb{R}, \tag{2.13}$$

where $E[\tilde{N}_{c_0}]$ can be replaced by its Monte Carlo estimate, namely $\widehat{E[\tilde{N}_{c_0}]}$.

Note that the null hypothesis, H_0, is tested versus an ensemble of alternative hypotheses H_{1r}, one for each value of θ_r fixed. The observed *sub-test statistics* $\{w(\theta_1), \ldots, w(\theta_R)\}$, realizations of $\{W(\theta)\}$, are combined into the global test statistic c_R, and an approximated bound for the global p-value is computed using (2.13). Thus, the problem of testing (1.2) is reduced to

testing H_0 versus the R *sub-alternative hypotheses* H_{1r}, that is, *testing one hypothesis multiple times.*

Cramér and Leadbetter (2013, p. 63 and 195) discuss adequate choices of Θ_R for which c, N_c, and $\sup_{\theta \in \Theta}\{W(\theta)\}$ are well approximated by c_R, $\tilde{N}_{c_R}$, and $\max_{\theta_r \in \Theta_R}\{W(\theta_r)\}$, respectively. However, in practice Θ_R may be determined by experiment. Therefore, in Section 3, we discuss graphical tools that can be used to assess whether these approximations hold.
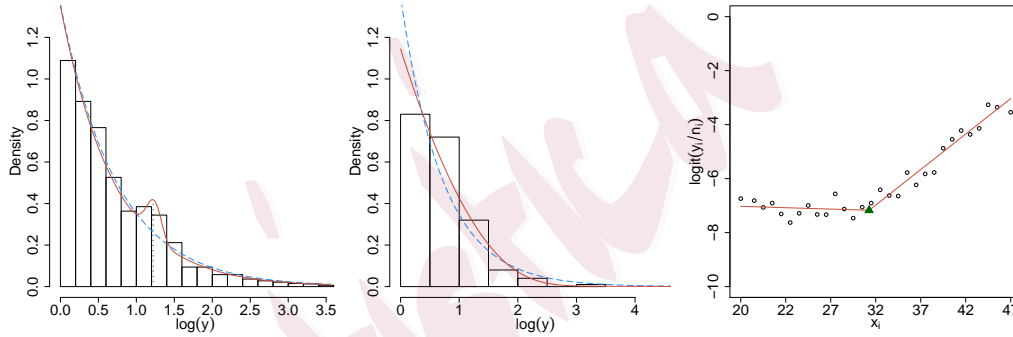

Figure 1: Data and fitted models. Left panel: histogram of the Fermi-LAT realistic data simulation for Example 1 (on log-scale), the null model (blue dashed curve) fitted under the assumption of background-only counts ($\hat{\phi} = 1.350$), and the fitted alternative model (red solid curve) with $\hat{\eta} = 0.045$ and $\hat{\phi} = 1.406$. The green dotted vertical line indicates the location of the observed Gaussian bump, i.e., $\hat{\theta} = 3.404$. Central panel: histogram of the Fermi-LAT realistic data simulation for Example 2 (log-scale), the null model when testing whether (1.2) is fitted as a power-law distributed cosmic source with $\hat{\phi} = 1.395$ (blue dashed curve). The null model when testing (3.16) is the dark matter model in (3.14) with $\hat{\theta} = 27.89$ obtained via MLE (red solid curve). Right panel: Down syndrome data and fitted regression model (red piecewise-linear solid lines), with break-point (green triangle) at $\hat{\theta} = 31.266$.

3. Practical matters

3.1 Case studies: Description

Here, we illustrate the implementation of TOHM in the context of three case studies: the "bump hunting" problem introduced in Section 1, a non-nested models comparison, and a logistic model with a break point. Hereafter, we refer to these as Examples 1, 2, and 3, respectively. The data for Examples 1 and 2 were generated using simulations of the Fermi Large Area Telescope (LAT), obtained using the *gtobssim* package, and include representations of detector effects and systematic errors. The Fermi-LAT is a γ-ray telescope on the orbiting Fermi satellite (Atwood et al., 2009).

In Example 1, our data analysis aims to properly distinguish between γ-ray signals induced by dark matter annihilations and those induced by the astrophysical background. As in (1.1), dark matter events are modeled as a Gaussian bump, with mean energy θ and standard deviation varying with θ. The astrophysical background is power-law (Pareto type-I) distributed, with index ϕ. In our simulation, we set $\theta = 3.5$ GeV (where GeV denotes Giga electron-volt), $\phi = 1.4$ and $\eta = 0.02$, and we consider the energy band $y \in [1; 35]$. This setup resulted in 64 dark matter events and 2274 background events. For more physics details, see Algeri et al. (2016).

http://fermi.gsfc.nasa.gov/ssc/data/analysis/software

In Example 2, the non-nested models to be compared are a dark matter

emission with probability density given by

$$g(y, \theta) \propto y^{-1.5} \exp\left\{-7.8\frac{y}{\theta}\right\}, \tag{3.14}$$

with $y \geq 1$, $\phi > 0$, and $\theta \geq 1$ (see Bergström et al., 1998), and a power-law

distributed cosmic source with density $f(y, \phi) \propto \frac{1}{k_\phi y^{\phi+1}}$. In our simulation,

we set the putative dark matter emission to occur at $\theta = 35$ GeV, and the

power-law index to $\phi = 1.4$. In this way, we obtained 200 dark matter

events over the energy band $y \in [1; 100]$.

Because the models $f(y, \phi)$ and $g(y, \theta)$ are non-nested, the classical

asymptotic properties of the MLE and LRT fail. However, as shown in

Algeri et al. (2016), the framework of Section 2 can be extended to compare

non-nested models by reformulating this comparison as a test in which a

nuisance parameter is identified only under H_1. Specifically, following Cox

(1962) and Atkinson (1970), we specify a comprehensive model that embeds

two non-nested models,

$$(1 - \eta)f(y, \phi) + \eta g(y, \theta) \qquad 0 \leq \eta \leq 1. \tag{3.15}$$

This reduces the problem to a nested models comparison, and we test (1.2).

However, in contrast to the bump-hunting example in (1.1), η has no physical interpretation in this case. Rather, as in Quandt (1974), η is an auxiliary parameter that allows us to exploit the normality of its MLE to apply well-known asymptotic results. In addition to (1.2), the hypotheses

$$H_0 : \eta = 1 \quad \text{versus} \quad H_1 : \eta < 1 \tag{3.16}$$

should be tested to exclude intermediate situations (e.g., Cox, 1962, 2013). That is, we want to avoid treating (3.15) as a mixture, and focus instead on comparing the two models. Testing both (1.2) and (3.16) is particularly suited to particle physics searches, where researchers typically assign different degrees of belief to the models being tested. Specifically, as described in van Dyk (2014), the most stringent significance requirements (e.g., Lyons, 2013, Table 1) are typically used only in the *detection* stage, that is, when testing (1.2) to assess the presence of a new signal. Conversely, in the *exclusion* stage, that is, when testing (3.16) to exclude the hypothesis of a signal being present, a significance level of 0.05 is typically sufficient. The Fermi-LAT data sets for Examples 1 and 2 are plotted in the first two panels of Figure 1. Both simulations are available in the Supplementary Material.

Finally, in Example 3 we consider the *Down syndrome dataset* available

in the R package `segmented` (Muggeo et al., 2008). The data set records whether babies born to 354,880 women are affected by Down syndrome. We use (3.17) to model the probability, π_i, that a woman of age x_i has a baby with Down syndrome, where $x_i \in [17; 47]$, and we let $\theta \in [20; 44]$. The logit of the ratio between the number of Down syndrome cases and number of births by age group is plotted in the right panel of Figure 1.

$$\log\left(\frac{\pi_i}{1-\pi_i}\right) = \phi_1 + \phi_2 x_i + \xi(x_i - \theta)\mathbb{1}_{\{x_i \geq \theta\}} \quad \forall i = 1, \ldots, n, \qquad (3.17)$$

where $\theta \in \mathbb{R}$ is the location of the unknown break-point. In this case, we test $H_0 : \xi = 0$ versus $H_1 : \xi \neq 0$.

In Example 1 and 2, we use the LRT, $T_n(\theta)$, as the sub-test statistic. Because both tests are of the form in (1.2), the test is on the boundary of the parameter space and, for each θ fixed, the asymptotic distribution under H_0 is a mixture of χ_1^2 and zero (Chernoff, 1954; Self and Liang, 1987), also known as a $\bar{\chi}$ distribution, which we dentote as $\bar{\chi}_{01}^2$. It can be shown (Algeri and van Dyk, 2019) that in this setting, the bound in (2.8) has the same form as that in the χ_1^2 case; that is, it is given by (1.5), with $s = 1$. In Example 3, we use the signed-root of the LRT $Q_n(\theta) = \text{sign}(\hat{\eta}_\theta - \eta_0)\sqrt{T_n(\theta)}$; hence, the sub-test statistics are asymptotically normally distributed under

H_0 (e.g., Davies, 1977).

3.2   The choices of c_0 and R

One way to select an appropriate threshold c_0 is to perform a sensitivity analysis based on few Monte Carlo simulations of the traces of the underlying processes under H_0. As discussed in Section 2, under suitable regularity conditions and when H_0 is true, the LRT and signed-root LRT processes $\{T_n(\theta)\}$ and $\{Q_n(\theta)\}$, respectively, converge uniformly to $\{W_\chi(\theta)\}$ and $\{Z(\theta)\}$, as $n \to +\infty$. More generally, given a test statistic $W_n(\theta)$ to be evaluated on the data $y_1, \ldots, y_n$ for each θ fixed, we write $\{W_n(\theta)\} \xrightarrow{d} \{W(\theta)\}$. Consequently, for each sample generated under H_0, we compute $\{W_n(\theta)\}$ over a fine grid of values of θ, which approximates $\{W(\theta)\}$ when n is large. In all our simulations, the nuisance parameters under the null model are estimated via MLE, and each simulated sample under H_0 is obtained using a parametric bootstrap (Efron and Tibshirani, 1994). We plot the results of our simulation in order to visualize the traces of $\{W_n(\theta)\}$, as shown in Figure 2 for Example 1. (Analogous plots for Examples 2 and 3 appear in Figure S.2.) In order to calculate (2.8), it is important to provide an accurate estimate of $E[N_{c_0}]$. Hence, we choose c_0 to be at a level (on the y-axis) around which the process $\{W_n(\theta)\}$ oscillates often and, thus, with respect to which the upcrossings occur with high frequency. For Examples 1, 2, and

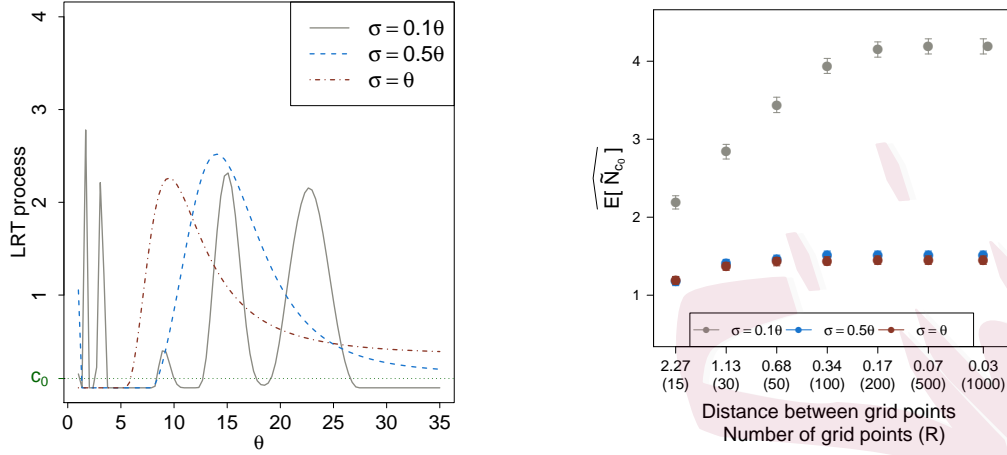## 3.2 The choices of c_0 and R

Figure 2: Left panel: simulated sample paths of the LRT process, $\{T_n(\theta)\}$, under H_0 in Example 1. Both plots consider different widths of the Gaussian bump. Right panel: upcrossings plot showing Monte Carlo estimates of $E[\tilde{N}_{c_0}]$ and standard errors (whiskers), under H_0, for Example 1, evaluated over grids of $R = 15, 30, 50, 100, 200, 500$ points, and for three choices of the Gaussian width, $\sigma = 0.1\theta, \sigma = 0.5\theta,$ and $\sigma = \theta$.

3, this leads to values of c_0 equal to $0.1, 0.3$, and 0, respectively. Inspecting the smoothness of the trace plots allows us to qualitatively assess Condition 1 and verify the goodness of the approximation of $E[N_{c_0}]$ by $E[\tilde{N}_{c_0}]$, which is necessary for the validity of the results of Section 2.

As discussed in Section 1, the implementation of our procedure requires that we specify of a grid Θ_R over $\Theta \equiv [\mathcal{L}; \mathcal{U}]$, where R is the number of times H_0 is tested versus the ensemble of sub-alternatives $H_{11}, \ldots, H_{1R}$. In practice, R must either be chosen arbitrarily by the researcher or be determined by the nature of the experiment. In either case, R must be sufficiently large to guarantee the robustness of the results, yet small enough

to ensure computational efficiency when calculating (2.13). One possibility is to choose R large enough so that, for a given c_0, $E[\tilde{N}_{c_0}]$ converges to a finite limit, which we expect, for sufficiently dense Θ_R, to correspond to $E[N_{c_0}]$. This strategy requires us to set c_0 before setting R.

In order to identify the value of R that best negotiates the trade-off between accuracy and computational efficiency, one can consider different values of R, and for each of them, compute an estimate of $E[N_{c_0}]$ using a small Monte Carlo simulation. The results can then be summarized in an *upcrossing plot*, where the values for R are reported on the x-axis, and the respective $\widehat{E[\tilde{N}_{c_0}]}$ estimates of $E[N_{c_0}]$ are reported on the y-axis. The upcrossing plot in the right panel of Figure 2 displays Monte Carlo estimates $\widehat{E[\tilde{N}_{c_0}]}$ for the LRT in Example 1, under H_0, as a function of R (with $R = 15, 30, 50, 100, 200, 500, 1000$). For each value of R considered, the grid points have been chosen to be equally spaced over Θ. Analogous plots for Examples 2 and 3 appear in Figure S.2. For each R considered, we computed 100 Monte Carlo simulations, each of size 1000. In all our examples, 100 simulations are sufficient to achieve small Monte Carlo errors.

As a rule of thumb, if the number of upcrossings increases with R, but does not converge, either the resolution is not sufficiently high to catch all the crossings, or the underlying process is not sufficiently smooth to

guarantee $E[N_{c_0}] < \infty$. Conversely, if the number of upcrossings converges, as in the well-known scree plot used for a principal component analysis (PCA) (e.g., James et al., 2013, p. 383), we look for an "elbow" in the plot of $\widehat{E[\tilde{N}_{c_0}]}$. The value of R corresponding to the elbow is the smallest value for which $\widehat{E[\tilde{N}_{c_0}]}$ converges to its limit, $E[N_{c_0}]$, up to the Monte Carlo error. In physics terms, this corresponds to the minimal value of R for which $\widehat{E[\tilde{N}_{c_0}]}$ well approximates the number of upcrossings of the underlying continuous time process.
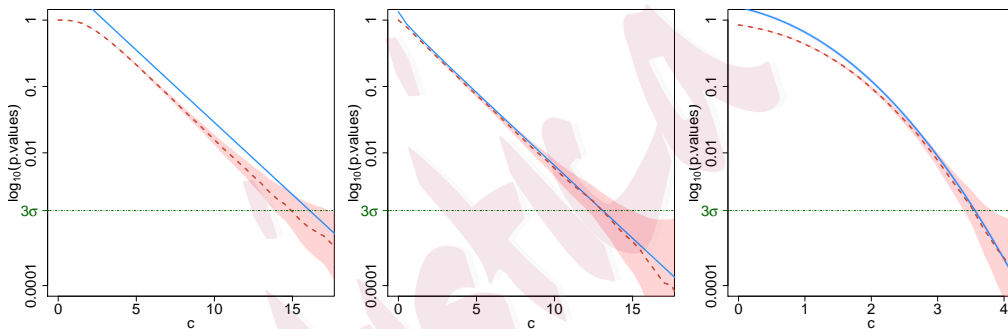

Figure 3: Estimated bound/approximation in (2.13) (blue solid line), simulated global p-values (on $\log_{10}$-scale), Monte Carlo estimates of $P(\sup_{\theta \in \Theta}\{W(\theta)\} > c)$ (red dashed line), and Monte Carlo errors (pink areas) for increasing values of the threshold c, for Example 1 (left panel), Example 2 (central panel), and Example 3 (right panel). Monte Carlo errors associated with $\widehat{E[\tilde{N}_{c_0}]}$ on the bound in (2.13) are plotted in gray, but are too small to be visible.

We also investigate the relationship between the width of the signal in the bump-hunting example and the grid resolution. In particular, we replicate the simulation for three choices of the Gaussian width, $\sigma = 0.1\theta, \sigma =$

0.5θ and $\sigma = \theta$. (In our actual analysis, $\sigma = 0.1\theta$.) As expected, wider

signals correspond to smoother underlying processes (Figure 2, left panel),

and $\widehat{E[\tilde{N}_{c_0}]}$ converges (Figure 2, right panel) at a lower grid resolution.

In general, R affects the upper bound/approximation for the global p-

value in (2.8) and the observed value of the test statistic, c_R, which we

assume converges to c as $R \to \infty$. Specifically, if the gap between θ_r and

θ_{r+1} is wider than the signal width, c_R may underestimate c, and the signal

may be missed. Thus, if the signal is suspected to be localized over a small

region of the search interval, a higher resolution is required to accurately

estimate (2.13) and avoid false negatives. This would, in turn, adversely

affect the power of the test.

Conversely, in Examples 2 and 3, the signal is spread either over the

whole parameter space or over a large portion of it. In these cases, the

choice of R should be based on the desired level of accuracy of both c_R, as

an estimate for the maximum of the underlying process, and θ, at which

the maximum occurs; that is,

$$\tilde{\theta} = \operatorname{argmax}_{\theta_r \in \Theta_R}\{W(\theta_r)\}. \tag{3.18}$$

Finally, based on the elbow in the upcrossing plots in Figures 2 and S.2,

the values of R we select are $R = 100$ in Example 1 (with $\sigma = 0.1\theta$, as in

(1.1)), $R = 50$ in Example 2, and $R = 30$ in Example 3. However, in order to

guarantee accuracy of at least 0.5 for the identified location, $\tilde{\theta}$, of the break-

point, we set $R = 50$ in Example 3. For each of the models considered, we

computed (2.13) using the R and c_0 selected above. The results obtained are

compared in Figure 3 with the Monte Carlo estimates of $P(\sup_{\theta \in \Theta}\{W(\theta)\} >$

$c)$ for increasing values of c, obtained using 100,000 simulations, each of size

10,000. The pink areas correspond to the respective Monte Carlo errors.

The Monte Carlo errors associated with the estimate $\widehat{E[\tilde{N}_{c_0}]}$ of $E[\tilde{N}_{c_0}]$ in

(2.13) (and displayed on a lower scale in the upcrossing plots) are also

incorporated in Figure 3, but they are too small to be visible. As expected,

the estimated TOHM bounds approach the "truth" as $c \to \infty$. Convergence

appears to be slower for Example 1. However, the plots are presented on

a $\log_{10}$-scale and, thus, in all cases, we obtain good approximations of the

global p-values.

4. Comparing TOHM and Bonferroni's bounds

In fields such as high energy physics and astrophysics, experiments are often

characterized by a search of one signal over a wide pool of possibilities. The

simplest possible way to tackle this problem using classical MHT is to use

Bonferroni correction (Bonferroni, 1935, 1936). The Bonferroni bound for

the global p-value is

$$p_{\mathrm{BF}} = R \cdot \min_{\theta_r \in \Theta_R} P(W(\mathcal{L}) \geq w(\theta_r)) = R \cdot P(W(\mathcal{L}) \geq c_R). \qquad (4.19)$$

The standard Bonferoni correction, p_{BF}, used to bound statistical signifi-
cance in multiple testing also yields a bound on $P(\max_{\theta_r \in \Theta_R}\{W(\theta_r)\} \geq c_R)$.
Specifically,

$$P\left(\max_{\theta_r \in \Theta_R}\{W(\theta_r)\} \geq c_R\right) = P\left(\cup_{\theta_r \in \Theta_R}\{W(\theta_r) > c_R\}\right) \leq \sum_{\theta_r \in \Theta_R} P(W(\theta_r) > c_R)$$

$$= R \cdot P(W(\mathcal{L}) > c_R) = p_{BF}.$$

In this section, we investigate the relationship between the TOHM and
Bonferroni bounds using simple constructs from EVT in order to individu-
ate situations where the latter can be used without leading to overly con-
servative results.

First, we introduce a distinction between upcrossings and *exceedances*
of $\{W(\theta_r)\}$. Specifically, an exceedance of c_R by $\{W(\theta_r)\}$ occurs at θ_r
if $\{W(\theta_r) > c_R\}$. An illustration of the difference between upcrossings
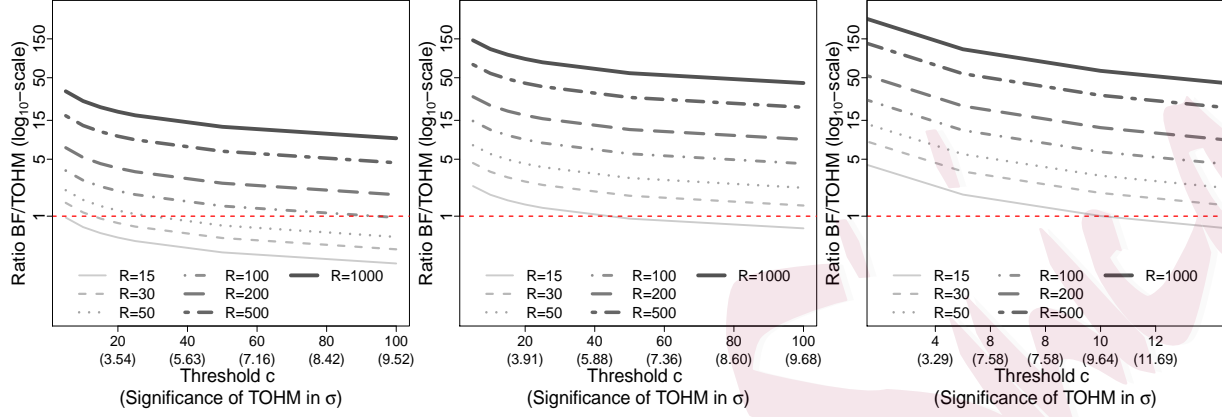and exceedances is given in Figure S.1. We denote by $\tilde{N}_{c_R}$ the process of

Figure 4: Ratio of Bonferroni and TOHM bounds at increasing values of c
(and corresponding significance for TOHM), and considering different resolu-
tions (gray curves). The left, central, and right panels correspond to Example 1,
2, and 3, respectively.

exceedances of c_R by $\{W(\theta_r)\}$, and let $\dot{N}_{c_R}$ be the process of upcrossings,

as defined in 2.3. Note that

$$E[\dot{N}_{c_R}] = \sum_{r=1}^{R} P\left(W(\theta_r) \geq c_R\right) = \sum_{r=1}^{R} P\left(W(\theta_r) \geq \max_{\theta_{r'} \in \Theta_R} \{w(\theta_{r'})\}\right) \quad (4.20)$$

$$= R \min_{\theta_r \in \Theta_R} P(W(\mathcal{L}) \geq w(\theta_r)) = p_{\mathrm{BF}}. \quad (4.21)$$

Because each upcrossing requires at least one exceedance, $E[\dot{N}_{c_R}] \geq$

$E[\tilde{N}_{c_R}]$. Moreover, we expect the clusters of exceedances corresponding to

each upcrossing to become smaller and, consequently, for $E[\dot{N}_{c_R}]$ to ap-

proach $E[\tilde{N}_{c_R}]$ as c_R increases. Here, $E[\dot{N}_{c_R}]$ can be computed easily using

p_{BF} in (4.20)-(4.21); whereas, when $\{W(\theta)\}$ satisfies Condition 1, $E[\tilde{N}_{c_R}]$ is

approximately equal to the second term in (2.13), for large R. Furthermore, $E[\tilde{N}_{c_R}]$ dominates the first term in (2.13) as $c_R \to \infty$. Thus, it is natural to consider if there are situations where (2.13) and p_{BF} are approximately equivalent bounds on $P(\max_{\theta_r \in \Theta_R}\{W(\theta_r)\} \geq c_R)$, that is

$$P(W(\mathcal{L}) > c_R) + \frac{a(c_R)}{a(c_0)} E[\tilde{N}_{c_0}] \approx p_{\text{BF}}, \qquad (4.22)$$

for $c_0 \leq c_R$, $c_R \to +\infty$, and $R \to +\infty$. Unfortunately, simultaneously quantifying the rates at which c_R and R must increase in order for (4.22) to hold is not an easy task. Hence, we investigate the approximation in (4.22) using a numerical simulation, where we compare the performance of the Bonferroni and TOHM bounds with respect to the number of tests considered and the level of significance for Examples 1, 2, and 3.

The results are reported in Figure 4, where we plot the ratio of the two bounds for increasing values of c using different grid sizes R. Because we use the signed-root LRT, $\{Q_n(\theta)\}$, in Example 3 rather than using the LRT, smaller values of c correspond to equally significant results. In the horizontal axes, the statistical significance is reported in terms of the σ-significance, that is, the number of standard deviations from the mean of a standard normal distribution that correspond to the tail probability

expressed by the one-sided p-value. In other words,

$$\#\sigma = \Phi^{-1}(1 - \text{p-value}),$$

where Φ is the standard normal cumulative function.

In Examples 2 and 3, Bonferroni is always more conservative than the TOHM bound when at least 30 tests are performed. For $R = 15$, Bonferroni becomes less conservative only when the level of significance achieved is of the order of 6σ and 11σ, respectively.

A more interesting situation is observed in Example 1. Here, the equivalence of p_{TOHM} and p_{BF} occurs for values of c much smaller than those for which the same limit is achieved in Examples 2 and 3. Furthermore, when $R \leq 50$, Bonferroni quickly becomes less conservative than the TOHM bound as c increases. For $R = 50$, for instance, Bonferroni outperforms TOHM when $c > 30$ ($\sim 4.5\sigma$ significance).

Finally, the plots in Figure 4 all suggest that the TOHM bound is preferable to Bonferroni with very high resolutions (i.e., $R \geq 500$) for all of the significance levels considered (up to $\sim 10\sigma$).

Note that the value of R selected using the upcrossing plots discussed in Section 3.2 is the minimum number of grid points (among those considered)

for which $\widehat{E[\tilde{N}_{c_0}]}$ converges to its limit. As R increases beyond this point, the estimated TOHM bound remains constant, whereas Bonferroni's bound continues to increase. Thus, when the number of tests to be conducted can be selected arbitrarly, Bonferroni will not be overly conservative if the "elbow" in the upcrossings plot appears at a relatively small value of R and the observed value of c is large. However, practitioners should keep in mind that when attempting to identify the signal location, $\tilde{\theta}$, a higher resolution is typically required and, thus, TOHM is preferable.

Example	Test	Method	R	c_R	$\tilde{\theta}$	p-value (Significance)
Example 1	$H_0 : \eta = 0$ $H_1 : \eta > 0$	Bonferroni TOHM	100	38.326	3.404	$2.99 \cdot 10^{-8}$ (5.42σ) $2.11 \cdot 10^{-8}$ (5.48σ)
Example 2	$H_0 : \eta = 0$ $H_1 : \eta > 0$ $H_0 : \eta = 1$ $H_1 : \eta < 1$	Bonferroni TOHM Bonferroni TOHM	50 50	21.021 0.606	27.265 27.890	$1.14 \cdot 10^{-4}$ (3.69σ) $2.51 \cdot 10^{-5}$ (4.06σ) > 1 $(0.00\sigma$ $)$ $7.201 \cdot 10^{-1}$ (0.58σ)
Example 3	$H_0 : \xi = 0$ $H_1 : \xi \neq 0$	Bonferroni TOHM	50	11.826	31.266	$1.43 \cdot 10^{-30}$ (11.43σ) $5.06 \cdot 10^{-31}$ (11.52σ)

Table 1: Summary of the results of TOHM and MHT via Bonferroni on real data for Examples 1, 2, and 3.

4.1   Data analyses

In this section, we compare the TOHM and Bonferroni bounds for Examples 1, 2, and 3. The results are summarized in Table 1. In the dark matter search problem of Example 1, we obtain significance in favor of the presence of a dark matter emission of about 5.4σ using both TOHM and MHT. This result is not surprising because $c_R = 38.326$ and, as shown in the central panel of Figure 4, at $c \approx 40$, the gray line associated with $R = 100$ is very close the red dashed line. The signal location selected is close to the truth (3.5 GeV), and the estimated model is plotted as a solid red line in the left panel of Figure 1; the signal location selected, $\tilde{\theta} = 3.404$, is indicated by the green dotted vertical line.

In Example 2, both TOHM and Bonferroni reject the hypothesis that the observed emission is due to a power-law distributed cosmic source at 4.06σ and 3.69σ, respectively. Because this example involves a non-nested model comparison, we invert the null of the hypotheses to avoid meaningless results (see Section 3.1 for more details). In the inverted test, the power-law model cannot be rejected. Both the fitted dark matter model and the fitted power-law cosmic source model are displayed in the central panel of Figure 1. In Example 2, when testing (1.2), the value of θ (i.e., the signal annihilation of the dark matter model) selected by TOHM is $\tilde{\theta} =$

27.265 GeV. This is somewhat off from the true value used to simulate the data ($\theta = 35$ GeV), perhaps because our analysis does not account for instrumental errors. Our analysis also only uses the spectral energy of the γ-ray signals, whereas, in practice, the directions of the γ-ray would also be used, thus increasing the statistical power.

Finally, for the break-point regression model in Example 3, both TOHM and MHT give similar inferences (11.52σ and 11.43σ, respectively) when rejecting the hypothesis of a linear model with no break-point. The equivalence between the two procedures is likely due to the high statistical significance and the moderately large number of tests conducted ($R = 50$). The fitted model is displayed in Figure 1, where the green triangle corresponds to the optimal break-point location; that is, the maximum of the signed-root LRT process occurs at a mother's age of 31.266 years.

5.   Conclusion

We have proposed a highly generalizable method to efficiently conduct statistical tests under nonstandard conditions, including bump-hunting, structural change detection, and a non-nested model comparison.

The main advantages of the proposed method are its easy implementation and its efficiency in providing an accurate inference, while controlling for very small type-I errors rates. Following Davies (1987) and Gross

and Vitells (2010), we combine the theoretical framework of EVT with the practical simplicity of Monte Carlo simulations, and generalize their results beyond the LRT and χ^2. Using several simulation studies, we show that as few as 100 Monte Carlo simulations are often sufficient to achieve a high level of accuracy. Although we do not investigate the power of TOHM here, interested readers are directed to Davies (1977) for a formal derivation of the lower and upper bounds of the power function in the normal case, and to the simulation studies conducted in Algeri et al. (2016) and Algeri et al. (2016) for the $\bar{\chi}^2_{01}$ case.

From a practical perspective, we propose simple graphical tools for selecting the threshold c_0 and for specifying an appropriate number of sub-tests R to guarantee the robustness of the resulting inference. Finally, we investigated the relationship between the TOHM and Bonferroni bounds, and implemented both procedures on our running examples. In future work, we will extend our results to the case where the nuisance parameter specified only under the alternative, $\boldsymbol{\theta}$, is multi-dimensional (Algeri and van Dyk, 2019).

Note that the stringent significance requirements play a critical role both in the theory discussed in Section 2 and in practical applications. Specifically, this setup is particularly well suited to searches in high energy

physics, where the significance level necessary to claim a discovery is at least 5σ. However, in light of the recent "p-value crisis," culminating in the journal *Basic and Applied Social Psychology* banning the use of the p-value in future submissions (Wasserstein and Lazar, 2016; Leek and Peng, 2015), stringent significance criteria may become more popular in other scientific communities.

Supplementary Material In Section S.1, we discuss the error rate of (2.8) for Gaussian, χ^2, and $\bar{\chi}^2_{01}$ processes. The proofs of Result 2 and Result 3 are collected in Section S.2. Additional figures are reported in Section S.3. Lastly, the data used in Examples 1 and 2 are provided.

References

Adler, R. (2000). On excursion sets, tube formulas and maxima of random fields. *Annals of Applied Probability*, 1–74.

Adler, R. and J. Taylor (2009). *Random fields and geometry*. Springer Science & Business Media.

Algeri, S. et al. (2016). On methods for correcting for the look-elsewhere effect in searches for new physics. *Journal of Instrumentation 11*(12), P12010.

Algeri, S., J. Conrad, and D. van Dyk (2016). A method for comparing non-nested models with application to astrophysical searches for new physics. *Monthly Notices of the Royal Astronomical Society: Letters 458*(1), L84–L88.

Algeri, S. and D. van Dyk (2019). Testing one hypothesis multiple times: The multidimensional case. *Journal of Computational and Graphical Statistics*, 1–14.

Anderson, B. et al. (2016). Search for gamma-ray lines towards galaxy clusters with the fermi-lat. *Journal of Cosmology and Astroparticle Physics 2016*(02), 026.

REFERENCES

Andrews, D. (1993). Tests for parameter instability and structural change with unknown change point. *Econometrica: Journal of the Econometric Society*, 821–856.

Andrews, D. and W. Ploberger (1994). Optimal tests when a nuisance parameter is present only under the alternative. *Econometrica: Journal of the Econometric Society*, 1383–1414.

Atkinson, A. (1970). A method for discriminating between models. *Journal of the Royal Statistical Society. Series B (Methodological)*, 323–353.

Atwood, W. B. et al. (2009). The large area telescope on the fermi gamma-ray space telescope mission. *The Astrophysical Journal 697*(2), 1071.

Bergström, L., P. Ullio, and J. Buckley (1998). Observability of γ rays from dark matter neutralino annihilations in the milky way halo. *Astroparticle Physics 9*(2), 137–162.

Bonferroni, C. (1935). Il calcolo delle assicurazioni su gruppi di teste. In *Studi in Onore del Professore Salvatore Ortu Carboni*, pp. 13–60. Rome.

Bonferroni, C. (1936). Teoria statistica delle classi e calcolo delle probabilità. *Pubblicazioni del R Istituto Superiore di Scienze Economiche e Commerciali di Firenze 8*, 3–62.

REFERENCES

Chernoff, H. (1954). On the distribution of the likelihood ratio. *The Annals of Mathematical Statistics*, 573–578.

Choudalakis, G. (2011). On hypothesis testing, trials factor, hypertests and the BumpHunter. In *Proceedings, PHYSTAT 2011. ArXiv:1101.0390.*

Cox, D. (1962). Further results on tests of separate families of hypotheses. *Journal of the Royal Statistical Society. Series B (Methodological)*, 406–424.

Cox, D. (2013). A return to an old paper:'tests of separate families of hypotheses'. *Journal of the Royal Statistical Society: Series B (Statistical Methodology) 75*(2), 207–215.

Cramér, H. and M. Leadbetter (2013). *Stationary and related stochastic processes: Sample function properties and their applications.* Courier Corporation.

Davies, R. (1977). Hypothesis testing when a nuisance parameter is present only under the alternative. *Biometrika 64*(2), 247–254.

Davies, R. (1987). Hypothesis testing when a nuisance parameter is present only under the alternative. *Biometrika 74*(1), 33–43.

REFERENCES

Davies, R. (2002). Hypothesis testing when a nuisance parameter is present
only under the alternative: linear model case. *Biometrika*, 484–489.

Efron, B. and R. Tibshirani (1994). *An introduction to the bootstrap*. CRC
press.

Gross, E. and O. Vitells (2010). Trial factors for the look elsewhere effect in
high energy physics. *The European Physical Journal C 70*(1-2), 525–530.

Hansen, B. (1991). Inference when a nuisance parameter is not identi-
fied under the null hypothesis. *Rochester Center for Economic Research
Working Paper No. 296*.

Hansen, B. (1992a). The likelihood ratio test under nonstandard condi-
tions: testing the markov switching model of gnp. *Journal of applied
Econometrics 7*(S1).

Hansen, B. (1992b). Testing for parameter instability in linear models.
Journal of policy Modeling 14(4), 517–533.

Hansen, B. (1996). Inference when a nuisance parameter is not identified
under the null hypothesis. *Econometrica: Journal of the econometric
society*, 413–430.

REFERENCES

Hansen, B. (1999). Threshold effects in non-dynamic panels: Estimation, testing, and inference. *Journal of econometrics 93*(2), 345–368.

Hotelling, H. (1939). Tubes and spheres in n-spaces, and a class of statistical problems. *American Journal of Mathematics 61*(2), 440–460.

James, G. et al. (2013). *An introduction to statistical learning*, Volume 112. Springer.

Leek, J. and R. Peng (2015). Statistics: P values are just the tip of the iceberg. *Nature 520*(7549), 612.

Lyons, L. (2013). Discovering the significance of 5 sigma. *arXiv preprint arXiv:1310.1284*.

Muggeo, V. et al. (2008). Segmented: an r package to fit regression models with broken-line relationships. *R news 8*(1), 20–25.

Quandt, R. (1974). A comparison of methods for testing nonnested hypotheses. *The Review of Economics and Statistics*, 92–99.

Rice, S. (1944). Mathematical analysis of random noise. *Bell Labs Technical Journal 23*(3), 282–332.

Self, S. and K.-Y. Liang (1987). Asymptotic properties of maximum likeli-

hood estimators and likelihood ratio tests under nonstandard conditions. *Journal of the American Statistical Association 82*(398), 605–610.

Taylor, J. and R. Adler (2003). Euler characteristics for gaussian fields on manifolds. *Annals of Probability*, 533–563.

Taylor, J. and K. Worsley (2008). Random fields of multivariate test statistics, with applications to shape analysis. *The Annals of Statistics*, 1–27.

van Dyk, D. (2014). The role of statistics in the discovery of a higgs boson. *Annual Review of Statistics and Its Application 1*, 41–59.

Wasserstein, R. and N. Lazar (2016). The asa's statement on p-values: context, process, and purpose.

Sara Algeri

School of Statistics

University of Minnesota

Minneapolis, MN, 55455

E-mail: salgeri@umn.edu

David van Dyk

REFERENCES

Statistics Section

Dept of Mathematics

Imperial College London

London, UK SW7 2AZ

E-mail: d.van-dyk@imperial.ac.uk